Check for updates

Novel "ruthenium cyclopentadienyl"–peptide conjugate complexes against human FGFR(+) breast cancer†

João Franco Machado, [ID] [a,b,c] Miguel Machuqueiro, [ID] [b,d] Fernanda Marques, [ID] [c] M. Paula Robalo, [ID] [e,f] M. Fátima M. Piedade, [ID] [b,e] M. Helena Garcia, [ID] [a,b] João D. G. Correia [ID] *[c] and Tânia S. Morais [ID] *[a,b]

In this work we explored the possibility of improving the selectivity of a cytotoxic Ru complex [RuCp (PPh$_3$)(2,2'-bipy)][CF$_3$SO$_3$] (where Cp = η^5-cyclopentadienyl) **TM34** towards FGFR(+) breast cancer cells. Molecular dynamics (MD) simulations of **TM34** in a phosphatidylcholine membrane model pinpointed the cyclopentadienyl group as a favorable derivatization position for the peptide conjugation approach. Three new Ru(II) complexes presenting a functionalized η^5-cyclopentadienyl were synthesized, namely [Ru(η^5-C$_5$H$_4$COOH)(2,2'-bipy)(PPh$_3$)][CF$_3$SO$_3$] (**TM281**) and its precursors, [Ru(η^5-C$_5$H$_4$COOCH$_2$CH$_3$)(η^2-2,2'-bipy)(PPh$_3$)][CF$_3$SO$_3$] (**3**) and [Ru(η^5-C$_5$H$_4$COOCH$_2$CH$_3$)(PPh$_3$)$_2$Cl] (**2**). Complex **TM281** was prepared by the hydrolysis of the ethyl ester group appended to the η^5-cyclopentadienyl ligand of complex **3** with K$_2$CO$_3$ in water/acetonitrile, followed by mild protonation using an ion exchange resin. The newly synthesized complexes were fully characterized by NMR, FTIR and UV-vis spectroscopic techniques. Also, electrochemical studies were carried out by means of cyclic voltammetry in order to evaluate the stability of the compounds. Single crystal X-ray diffraction studies were carried out for compounds **3** and **TM281** which crystallized in the monoclinic system, space group *P*21/*n*. The unprecedented synthesis and characterization of three half-sandwich ruthenium(II)-cyclopentadienyl peptide conjugates and their preliminary biological evaluation against human FGFR(+) and FGFR(−) breast cancer cells are also reported.

^{a}*Centro de Química Estrutural, Faculdade de Ciências, Universidade de Lisboa, Campo Grande, 1749-016 Lisboa, Portugal. E-mail: tsmorais@ciencias.ulisboa.pt*
^{b}*Departamento de Química e Bioquímica, Faculdade de Ciências, Universidade de Lisboa, Campo Grande, 1749-016 Lisboa, Portugal*
^{c}*Centro de Ciências e Tecnologias Nucleares e Departamento de Engenharia e Ciências Nucleares, Instituto Superior Técnico, Universidade de Lisboa, Estrada Nacional 10 (km 139, 7), 2695-066 Bobadela LRS, Portugal.*
E-mail: jgalamba@ctn.tecnico.ulisboa.pt
^{d}*BioISI - Biosystems & Integrative Sciences Institute, Faculdade de Ciências da Universidade de Lisboa, Campo Grande, 1749-016 Lisboa, Portugal*
^{e}*Centro de Química Estrutural, Instituto Superior Técnico, Universidade de Lisboa, Av. Rovisco Pais, 1049-001 Lisboa, Portugal*
^{f}*Área Departamental de Engenharia Química, Instituto Superior de Engenharia de Lisboa, Instituto Politécnico de Lisboa, Rua Conselheiro Emídio Navarro 1, 1959-007 Lisboa, Portugal*
†Electronic supplementary information (ESI) available. CCDC 1578875 and 1578876. For ESI and crystallographic data in CIF or other electronic format see DOI: 10.1039/D0DT00955E

Introduction

Cancer is one of the leading causes of death worldwide. In 2018, 1 in 6 deaths was caused by cancer, which represents a total of 9.6 million deaths.[1] Breast cancer is the most common cancer in women, with a new case emerging every 20 seconds and one death every minute.[2,3] Although most of the breast cancer subtypes (positive for estrogen, ER, progesterone, PR, and/or human epidermal growth factor 2, HER2 receptors) can respond to hormone therapy when detected early, the highly metastatic triple negative breast cancer subtype (characterized by the absence of these three receptors) has a poor prognosis, even if diagnosed early, being responsible for most breast cancer deaths.[4] Currently, therapeutic strategies for cancer control include surgery and conventional cytotoxic treatments such as radiation therapy and chemotherapy. However, the latter presents low therapeutic indices and a wide spectrum of severe side effects, since most drugs in clinical use display little or no selectivity.[5–7] Another setback in cancer therapy is the development of drug and multi-drug resistance, which can be due also to limited tumor penetration.[8] Therefore, the development of new anticancer drugs based on novel modes of action with improved cancer cell selectivity is urgently needed.

In the last two decades, research on metal-based drugs has made remarkable progress in cancer therapy. Although most of the research efforts have been directed towards cisplatin

and its derivatives, which are still widely used to treat numerous cancers, particularly malignant solid tumors like testicular cancer, ovarian cancer, esophageal cancer, bladder cancer, head and neck cancer, and small-cell lung carcinoma,[9] research in this field has also been extended to include a noticeable number of non-platinum metallodrugs. Great attention has been paid to ruthenium compounds due to their important antitumor activities and to several advantages over platinum drugs, such as low toxicity and lower drug resistance, and thus they are likely to become a new generation of metal anticancer drugs with clinical importance.[10–12] In this direction, and to mention a few, two ruthenium coordination compounds NAMI-A ([ImH][*trans*-Ru(III)Cl$_4$Im(M$_{e_2}$SO)]; Im = imidazole) and KP1019 ([Hind][*trans*-Ru(III)Cl$_4$(Ind)$_2$], Ind = indazole) are under clinical trials against metastatic and colon cancers, respectively.[13] Nevertheless, coordination compounds present some drawbacks concerning the clinical applications due to their instability and complex ligand exchange chemistry. Organometallic chemistry appears to be an attractive alternative in clinical research to obtain organo-ruthenium complexes as suitable drug candidates. Numerous organometallic 'ruthenium(II)-(η^6-C$_6$H$_6$)'/(η^6-C$_6$H$_5$R)' complexes exhibiting antitumor properties against a wide variety of tumor types have been reported,[14–16] with some of the complexes being active in cisplatin-resistant cell lines.[17] Under this framework, we pioneered the report of the strong cytotoxic activity against colon (LoVo) and pancreas (MiaPaca) cancer cell lines of two half sandwich cationic complexes derived from the "Ru(η^5-C$_5$H$_5$)" fragment.[18] In the last few years, we have enlarged this family of compounds, which presented cytotoxic activities in the nano- and sub-micromolar ranges in several cancer human cell lines. Most of these compounds are more potent than cisplatin and, notably, they are also active in cell lines resistant to cisplatin.[19–30] The main targets of these ruthenium complexes are located in the cell membrane, mitochondria and Golgi apparatus, unlike the platinum drugs whose main target is DNA.[20,26–28,30] One of these compounds (**TM90**) was evaluated in an orthotopic metastatic triple negative breast cancer mouse model and was able to suppress tumor growth, without the observable side-effects of other non-targeted drugs.[31] Contrary to the control groups, metastasization was avoided and no signs of injury were found in the lungs, kidney, liver and spleen of the treated mice.[31]

Biologically active peptides have been increasingly explored as drug vectoring systems for targeting tumors, allowing an increase in selectivity and, consequently, leading to reduced toxicity.[32,33] The overexpression of specific receptors for these peptides in cancer cells compared to healthy cells from which they are derived enables their preferential binding and accumulation in tumor cells. In addition, peptides are endogenous molecules in the human body that tend to be less toxic and recognize their receptors selectively and with high affinity.[33] The fibroblast growth factor receptor (FGFR) is overexpressed in triple-negative breast cancer cells and is a marker associated with poor prognosis, early relapse and metastasis.[33] This receptor is subdivided into four subtypes (FGFR1 to FGFR4), with different expression patterns in breast cancer cells. The four receptor variants have been extensively studied and there is already a large number of ligands known to be specific (either peptides or small molecules) for each of them (except for subtype 4).[34–36] Therefore, FGFR-targeting peptides may be considered as promising carriers for selective tumor targeting.

Encouraged by our previous results obtained with the compound [RuCp(PPh$_3$)(2,2′-bipy)][CF$_3$SO$_3$] (where Cp = η^5-cyclopentadienyl) **TM34**[26,27,29,37] that showed excellent anticancer properties, we explored the possibility of improving its selectivity by conjugation to targeting peptides. In the work described herein, we used molecular dynamics (MD) simulations of **TM34** inserted in a phosphatidylcholine membrane to evaluate the most promising positions to derivatize the complex and help guide the experimental efforts. Hence, we report the synthesis and characterization of three new ruthenium(II) complexes (**2**, **3**, and **TM281**) analogous to **TM34** but differing in the cyclopentadienyl derivatization used as precursors of the following syntheses of the conjugate complexes. In fact, modification of the cyclopentadienyl ring can be a powerful tool in drug design, allowing the conjugation of a peptide that can constitute a vector for targeting tumors. Herein, we also report the unprecedented synthesis and characterization of three half-sandwich ruthenium(II)-cyclopentadienyl peptide conjugates (**RuPC1**, **RuPC2** and **RuPC3**) and their preliminary biological evaluation against human FGFR(+) and FGFR(−) breast cancer cells. In this work, three small peptides with 12 amino acid residues (**Pep1**: GPPDWHWKAMTH, **Pep2**: SRRPASFRTARE and **Pep3**: VSPPLTLGQLLS),[34,38–40] each one specific for targeting a receptor subtype (FGFR1 to FGFR3), were selected and conjugated to the complex [Ru(η^5-C$_5$H$_4$COOH)(PPh$_3$)(2,2′-bipy)][CF$_3$SO$_3$] (**TM281**) using a PEG polymer as a spacer group.

Results and discussion

MD simulations of TM34 interacting with a membrane model

Considering that the main targets of the above-mentioned ruthenium complexes that lead to the antiproliferative action are mainly located on the cell membrane, it is important to determine which part of the molecules is less affected in terms of its ability to interact with the membrane upon derivatization with a targeting moiety, namely a FGFR-targeting peptide.

With this goal in mind, we performed molecular dynamics (MD) simulations of the **TM34** complex interacting with a phosphatidylcholine bilayer to investigate which are the preferred membrane regions sampled by the complex (Fig. 1, left). In all replicates, under 200 ns, **TM34** inserts into the membrane and accumulates in a region ~7 Å below the average phosphate positions. The absence of membrane exit or crossing events indicates that this position is indeed a significant energy minimum. The structural representation at the end of the first replicate (Fig. 1, right) highlights the membrane
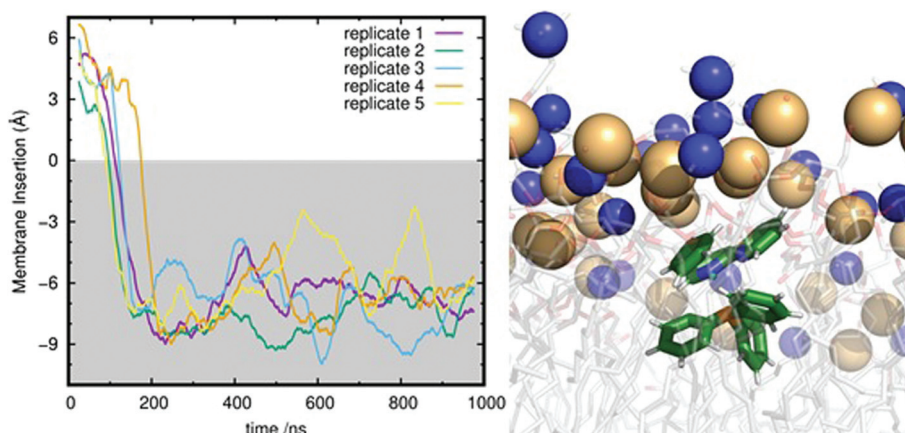
Fig. 1 Membrane insertion profiles of **TM34** over time (left) and structural representation of the complex deeply inserted into the DMPC membrane. The zero reference for the membrane insertion was calculated from the average along the membrane normal of the phosphorus atoms in the interacting monolayer. The snapshot corresponds to the final conformation of replicate 1. The DMPC lipid structures are shown with transparent grey sticks and spheres on the phosphorus (orange)/nitrogen (blue) atoms. The **TM34** complex is shown as thicker green sticks.

depth of this preferred location. We also analyzed membrane perturbation due to the presence of the complex, both in the head group (membrane thickness) and in the lipid tails (lipid tail order parameter), to find out whether these properties were unaltered (within the error bars) compared with simulations of pure DMPC (data not shown).

Since **TM34** has a strong preference for interacting with lipid bilayers, it becomes highly relevant to investigate how the complex orients itself along the membrane normal. This information can help us identify which coordinating groups in the molecule are more water accessible, and hence, the ones that could be derivatized without a major impact on the drug/membrane interaction. From the MD simulations of the equilibrated segments (after the complex inserts into the membrane), we calculated the angles of three vectors with the membrane normal, one per Ru-coordinating group (Fig. 2), namely: Ru···P of triphenylphosphine (Ph); Ru···⟨C⟩ of the

average position of the 5 carbon atoms in the cyclopentadienyl group (Cp); and Ru···⟨N⟩ of the average position of the 2 nitrogen atoms in the bipyridyl group (2,2′-bipy). The calculated angles for the three groups show a clear orientation preference where the Ph group mostly faces inwards into the lipid tails. The histogram peak at ∼30° probably corresponds to the best tilt which allows for lipid intercalation of the three phenyl groups. The simulations also indicate that there is no significant difference in the orientations of 2,2′-bipy and Cp which are always more accessible to the water phase (peaks at ∼120°). Combined together, these results indicate that derivatizations on either 2,2′-bipy or Cp should not perturb the membrane interaction abilities of the **TM34** based molecules as much as chemically modifying the Ph phenyl groups. Therefore, and aligned with the objectives of this work, we will proceed with the chemical modification of the cyclopentadienyl group.
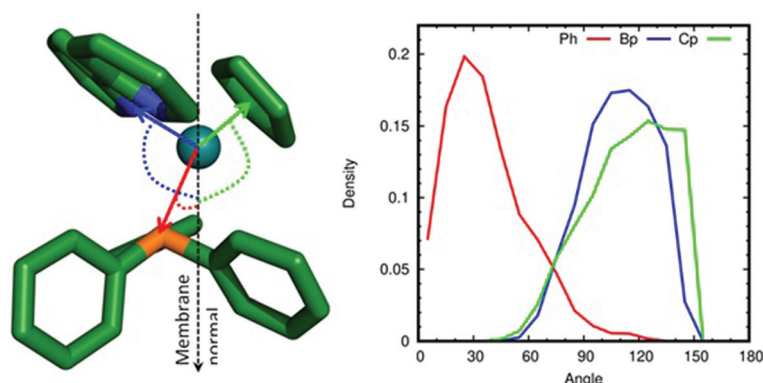

Fig. 2 Orientation of the three Ru-coordinating groups in **TM34** along the membrane normal. The vectors are defined starting from the ruthenium atom (left panel) and ending in the phosphorus atom of triphenylphosphine (Ph in red), the geometrical center of the two nitrogen atoms in the bipyridyl (2,2′-bipy – **Bp**- in blue), and the geometrical center of cyclopentadienyl (**Cp** in green). The calculated angles for the three groups are shown as normalized histograms (right panel).

## Synthesis and characterization of the organometallic precursors

The reaction between sodium cyclopentadienyl and diethyl carbonate in THF solution produces sodium carbethoxycyclopentadienyl (**1**, Scheme 1) in a high yield following the procedure described in the literature.[41] Treatment of $RuCl_2(PPh_3)_3$ with freshly prepared sodium carbethoxycyclopentadienide (**1**) in THF at room temperature leads to a new organometallic compound, formulated as $[Ru(\eta^5-C_5H_4COOCH_2CH_3)(PPh_3)_2Cl]$ (**2**), presenting the Cp ring functionalized with an ester group $-COOCH_2CH_3$. Chloride abstraction of this compound opens the way for the synthesis of several families of organometallic compounds by the use of either monodentate or bidentate ligands. In the present case, a new cationic complex $[Ru(\eta^5-C_5H_4COOCH_2CH_3)(PPh_3)(2,2'-bipy)][CF_3SO_3]$ (**3**) was prepared by chelation of 2,2′-bipyridine, with silver triflate being used as the abstractor reagent (Scheme 1). This reaction was carried out at reflux in methanol, and the resulting compound was recrystallized, at room temperature, by slow diffusion of diethyl ether in a dichloromethane solution. Hydrolysis of the ethyl ester group appended to the Cp ring with K_2CO_3 in compound **3** followed by acidification with an ion exchange resin leads to the compound $[Ru(\eta^5-C_5H_4COOH)(PPh_3)(2,2'-bipy)][CF_3SO_3]$ (**TM281**), bearing the carboxylic acid group (Scheme 1). It is important to stress that the use of the ion exchange resin instead of a strong inorganic acid is fundamental for the success of this reaction. In fact, the synthesis of the carboxycyclopentadienyl complex is a very difficult task; we start with the reaction of Thiele's acid with $Ru(PPh_3)_3Cl_2$ in toluene or DMF, and no reaction was observed, with the Thiele's acid dimer starting material being always recovered. Then our strategy was focused on the ester hydrolysis methodology. Many attempts for the hydrolysis of compound **3** with KOH, LiOH, NaOH, and K_2CO_3 in methanol, ethanol and THF

failed. The treatment of compound **3** with K_2CO_3 in a mixture of water/acetonitrile gave an orange solution of the complex $[Ru(\eta^5-C_5H_4COOK)(PPh_3)(2,2'-bipy)][CF_3SO_3]$, however under acidic conditions (HCl) the decomposition of the complex was observed. This problem was solved by the addition of an ion exchange resin Amberlite® to the $[Ru(\eta^5-C_5H_4COOK)(PPh_3)(2,2'-bipy)][CF_3SO_3]$ solution, instead of a strong acid, affording a red solution of $[Ru(\eta^5-C_5H_4COOH)(PPh_3)(2,2'-bipy)][CF_3SO_3]$ (**TM281**).

The three-new ruthenium derived compounds were fully characterized by FTIR, UV-vis, and ^1H-, ^{13}C-, ^{31}P-NMR spectroscopic techniques. The percentage elemental analyses of the complexes were in accordance with the proposed formulations. The electrochemical properties of these new compounds were studied by means of cyclic voltammetry. The structures of compounds **3** and **TM281** were also characterized by single crystal X-ray diffraction studies. The solid state FTIR spectra of all complexes present the characteristic bands of the functionalized cyclopentadienyl ligand and phenyl aromatic rings in the region of 3040–3100 cm^{-1}, with $\nu_{C=C}$ vibrations appearing at 1419–1479 cm^{-1} and $\nu_{C=O}$ vibrations in the range of 1701–1708 cm^{-1}. Compounds **3** and **TM281** also presented the vibration of the $CF_3SO_3^-$ anion at ~1280–1263 cm^{-1}. For compound **TM281**, the vibration of –OH of carboxylic acid in the range of 3040–3100 cm^{-1} was observed as well.

NMR spectroscopic characterization

^1H-, ^{13}C- and ^{31}P-NMR experiments were complemented by 2D experiments (COSY, HMQC and HMBC) in acetone-d^6 and chloroform-d solutions for the complete characterization of the new ruthenium(II) compounds. Scheme 1 shows the numbering of the coordinated 2,2′-bipyridyl ligand and the η^5-cyclopentadienyl rings for simplicity of the present discussion and the relevant ^1H-NMR data are gathered in Table S1.†
^1H-NMR spectra revealed a pattern of resonances characteristic of the monosubstituted η^5-cyclopentadienyl ring (Cp′ = C_5H_4R with R = $-COOCH_2CH_3$; $-COOH$) in the expected range for monocationic ruthenium(II) complexes. Comparison of complexes **2** and **3** reveals an expected deshielding of the η^5-Cp′ ring protons by 1.11 ppm for H_γ and 0.41 ppm for H_β due to the formation of a cationic complex. The same effect was also found for compound **TM281** with these deshieldings being 1.15 ppm and 0.69 ppm respectively. Thus, a large electronic asymmetry is created on the Cp ring due to the appended $-COOCH_2CH_3$ and $-COOH$ acceptor groups. Comparison of the NMR spectra of complexes **2** and **3** also shows a slight shielding of the protons of the ester group appended to the η^5-Cp′ ring (0.12 ppm for CH_2 and 0.29 ppm for CH_3) possibly due to the interaction with the 2,2′-bipyridyl rings. The effect of coordination on 2,2′-bipyridyl protons is observed by the significant shielding of H1 protons (0.56 ppm for compound **3** and 0.37 ppm for compound **TM281**) as also found for **TM34** (H1 was shielded by 0.34 ppm) for which this shielding was attributed to π-back donation from d_{Ru} to $\pi^*_{bipyridyl}$ orbitals.[37] Therefore, an electronic flow from the ruthenium center to the ligand through the coordinated nitrogen atoms also contrib-
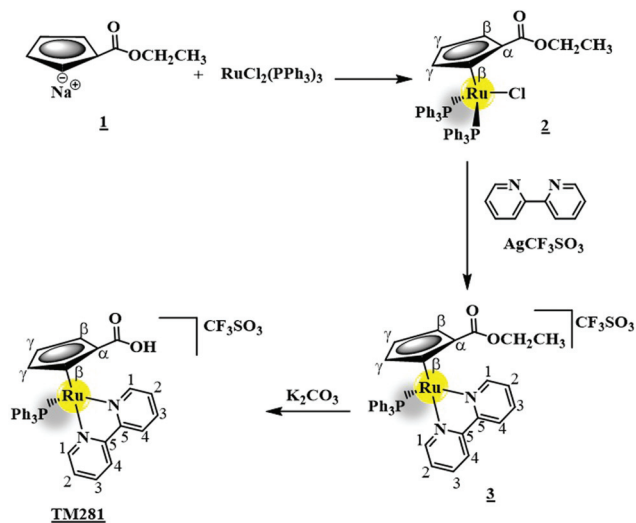
Scheme 1 Reaction scheme for the synthesis of Ru(II) complexes with the numbering scheme for NMR purposes.

utes to the significant electronic asymmetry of the 2,2′-bipyri-dyl coordinated ligand. The overall effect of this asymmetric distribution of charges in the Cp′ and 2,2′-bipyridyl can impart important reactivity to these compounds. This electronic asymmetry could be significant in the molecular interactions with anionic cell membranes since various anionic molecules are more abundant on the surface of cancer cells compared to healthy cells.[6,8] In addition, ^{13}C-NMR and ^{31}P-NMR spectroscopic studies were in good agreement with the results presented above. ^{13}C-NMR spectra revealed, upon coordination of the heteroaromatic ligand, the same general effect observed for the protons. The ^{31}P-NMR spectra of complex **2** show a single sharp signal for the triphenylphosphane coligand at ~37 ppm and an expected deshielding upon coordination of the 2,2′-bipyridyl ligand (compounds **3** and **TM281**) to ~50 ppm. In fact, the effect of π back donation Ru → 2,2′-bipyridyl will drive electronic density from triphenylphosphane to the Ru center.

Electronic absorption spectroscopy

The electronic absorption spectra of the three newly synthesized ruthenium complexes were recorded in ~5 × 10^{-5} mol dm^{-3} solutions of dichloromethane and the corresponding maximum absorption bands are indicated in Table S2.† For comparison, also the electronic spectrum of free 2,2′-bipyridine was obtained under the same experimental conditions. All ruthenium(II) complexes showed intense absorption bands in the UV region, in the range of 235–335 nm, attributed to electronic transitions occurring in the organometallic fragment $\{Ru(\eta^5-C_5H_4R)(PPh_3)\}^+$ (R = COOCH$_2$CH$_3$ or COOH) and the coordinated 2,2′-bipyridyl ligand. In addition to these bands, two maximum absorptions between 400 nm and 500 nm were found for compounds **3** and **TM281**, assigned to metal ligand charge transitions (MLCTs) from d$_{Ru}$ to π* orbitals centered on N coordinated atoms of the 2,2′-bipyridyl ligand, in accordance with our NMR data. Fig. 3(a) gathers the spectra of $[Ru(\eta^5-C_5H_4COOCH_2CH_3)(PPh_3)(2,2′-bipy)][CF_3SO_3]$ **3**, the starting compound $[Ru(\eta^5-C_5H_4COOCH_2CH_3)(PPh_3)_2Cl]$ **2** and the free ligand 2,2′-bipyridyl for comparison. It is clear that the coordination of 2,2′-bipyridyl leads to an enhancement of the main band placed at ~285 nm, attributed to a π → π* transition, the corresponding ε value being increased to 11 × 10^3 M^{-1} cm^{-1}. This finding is in good agreement with our ^{1}H-NMR data which reveal a shielding of 0.56 ppm for the 2,2′-bipyridyl *ortho* protons (H1) after coordination, as a consequence of the significant electronic flow towards this ligand. The presence of the MLCT band at 414 nm (ε = 6.5 × 10^3 M^{-1} cm^{-1}) corroborates this observation. In Fig. 3(b) we find the comparison between complexes **3** and **TM281** and we observe that both bands, π → π* of 2,2′-bipyridyl transition and MLCT, fade for compound **TM281** as would be expected by the lower shielding of the 2,2′-bipyridyl *ortho* protons (0.37 ppm).

Electrochemical studies

The redox behavior of the compounds was studied by cyclic voltammetry in dichloromethane and acetonitrile solutions
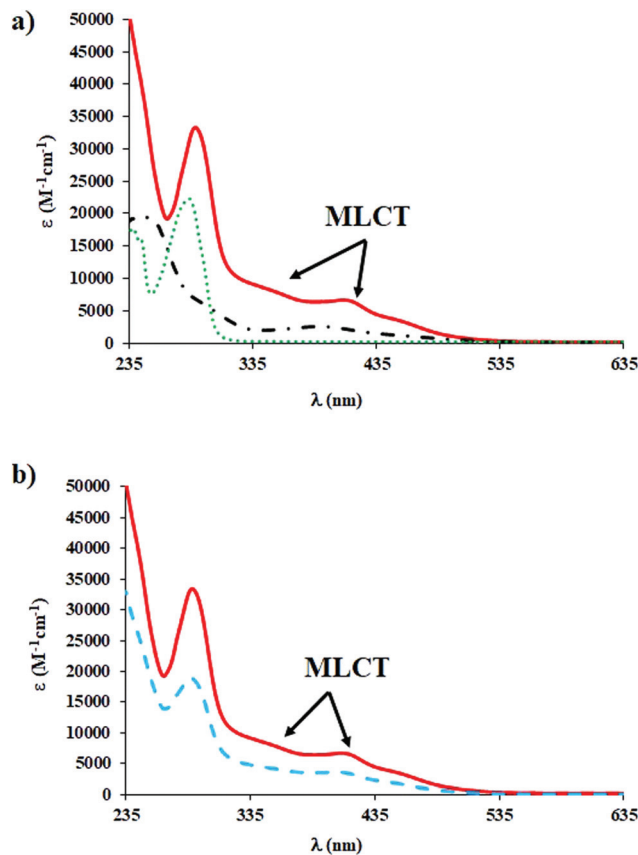

Fig. 3 Electronic spectra of (a) [Ru(η^5-C$_5$H$_4$COOCH$_2$CH$_3$)(PPh$_3$)(2,2′-bipy)][CF$_3$SO$_3$] (red solid line), [Ru(η^5-C$_5$H$_4$COOCH$_2$CH$_3$)(PPh3)$_2$Cl] (dot-dashed line) and 2,2′-bipy (green dotted line); (b) [Ru(η^5-C$_5$H$_4$COOCH$_2$CH$_3$)(PPh$_3$)(2,2′-bipy)][CF$_3$SO$_3$] (red solid line), [Ru(η^5-C$_5$H$_4$COOH)(PPh$_3$)(2,2′-bipy)][CF$_3$SO$_3$] (blue dashed line) in ~5 × 10^{-5} M dichloromethane solutions.

containing ammonium hexafluorophosphate as the supporting electrolyte between the limits imposed by the solvents (Table S3†) in order to evaluate the electronic richness at the active-redox centers and the reversibility of the oxidation/reduction processes. The study of the reversibility of the redox processes gives an insight into the stability of the oxidized and/or reduced species and knowledge of metal-centered redox potentials can provide a powerful tool for the design of new complexes and a better understanding of the role of metallodrugs in biological applications. In a 0.2 M [n-Bu$_4$N][PF$_6$]/dichloromethane solution, complex **2** was redox-active showing a quasi-reversible ruthenium centered process at $E_{1/2}$ = 0.61 V, followed by one irreversible wave (E_{pa} = 1.49 V), attributed to ligand centered oxidation. This complex was not studied in acetonitrile due to its insolubility in this solvent. In the case of complex **3** the electrochemical behavior in dichloromethane was characterized by a ruthenium centered process (oxidation) at 1.31 V with an i_{pc}/i_{pa} ratio of 0.6, suggesting some instability of the oxidized ruthenium species at the electrode surface (Fig. 4). Scan rate studies showed that it became more reversible when the scan direc-
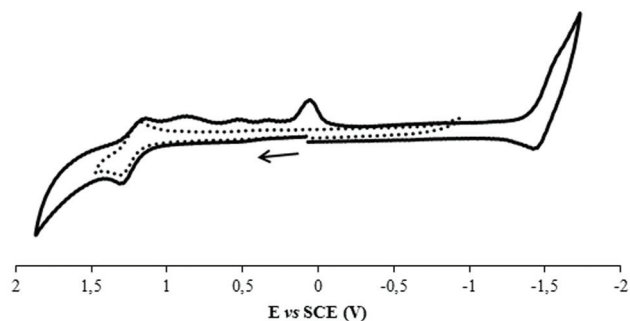
Fig. 4 Cyclic voltammogram of complex **3** in CH_2Cl_2, at 200 mV s^{-1}, showing the reversibility of the isolated oxidative processes (dashed line).
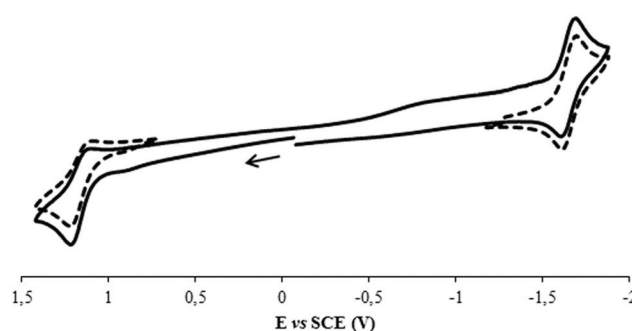

Fig. 5 Cyclic voltammogram of complex **TM281** in CH_3CN, at 200 mV s^{-1}, showing the reversibility of the isolated oxidative processes: both ligand and Ru^{II}/Ru^{III}.

tion was immediately reverted after applying the oxidation potential at high scan rates (1000 mV s^{-1}). In contrast, at a lower scan rate (50 mV s^{-1}) the process became more irreversible. This behavior can be associated with Ru^{II}/Ru^{III} oxidation, followed by fast decomposition. At higher scan rates, the scan direction is reversed before an appreciable amount of decomposition occurred. The presence of small irreversible reduction waves, dependent on the scan reverse at higher potential values (see Fig. 4), is probably related to the decomposition products. The oxidation potential value found for $[Ru(\eta^5\text{-}C_5H_4COOCH_2CH_3)(PPh_3)(2,2'\text{-bipy})][CF_3SO_3]$ is slightly higher than the one found for the related $[Ru(\eta^5\text{-}C_5H_5)(PPh_3)(2,2'\text{-bipy})][CF_3SO_3]$ **TM34** complex ($E_{pa} = 1.10$ V)[37] under the same experimental conditions (see Table S3†), indicating that the substitution of the cyclopentadienyl ring by the electron withdrawing ester group probably influences the electronic capability of the ruthenium(II) center, making the oxidation process more difficult.

The electrochemical response of the complex in acetonitrile is consistent with the behavior found in dichloromethane. Substitution of the ester by a carboxylic acid group in the cyclopentadienyl ring leads to a similar electrochemical behavior for complex **TM281** in dichloromethane. Nevertheless, in acetonitrile, the redox response is quite different, with the presence of two quasi-reversible redox processes, one at positive potentials ($E_{1/2} = 1.16$ V) attributed to the Ru(II)/Ru(III) couple and another ligand-based process at negative potentials ($E_{1/2} = -1.64$ V) (Fig. 5). The apparent redox stability of compound **TM281**, either at the metal center or at the coordinated 2,2′-bipyridine ligand, points toward some stability of the Ru-peptide conjugates. In fact, these conjugates were found to be very stable during preparation and manipulation (see below).

Crystal structures of complexes 3 and TM281

Single crystals of complexes **3** and **TM281** suitable for SCXRD were obtained by slow diffusion of diethyl ether in a dichloromethane solution. Both compounds crystallized in the monoclinic system, space group $P2_1/n$. The molecular structures of the cations of these complexes are shown in Fig. 6 along with the relevant atomic notation adopted. Selected bond lengths

and angles are presented in Table S4.† These monocyclopentadienyl complexes of ruthenium present the usual "three-legged piano stool" geometry around the metal as confirmed by N–M–P angles close to 90° (see Table S4†) with the remaining Cp–M–X (with X = N or P) angles between 124.38(2)° and 131.41(5)°. The values of bond lengths and angles are comparable to the ones found in the similar structure of **TM34**.[37] The angle between the plane formed by the carbethoxycyclopentadienyl moiety and the plane formed by bipyridine in compound **3** is wider (60.23°) than that in compound **TM281** (47.09°), because of the stereochemical hindrance of the bulkier derivative in the Cp ligand. For the same reason the bipyridine ligand in **3** is slightly more planar than that in **TM281**; the angle between the two pyridines is 5.74° in **3** while in **TM281** it is 6.74°.

The molecular packing of both complexes is very similar. The cation of compound **3** is enclosed by 3 anions and 5 cations. Table S5† shows the values of the distances of the intermolecular interactions for the two compounds. Crystal packing of compound **3** is formed by chains of cations intercalated by anions along the b axis that are sustained by C24–H24⋯O2 (2.39 Å), C4–H4⋯O3 (2.52 Å) and C112–H112⋯O2 (2.61 Å) intermolecular interactions (Fig. 7a). These chains are propagated along the a axis by the non-classical hydrogen bond C1–H1⋯O1 (2.57 Å) (Fig. 7b). The overall packing is completed by C–H⋯π interactions (C113–H113⋯π; centroid of the phenyl ring (C121–C216), 2.70 Å) (Fig. 7c).

In compound **TM281** the cation interacts with 7 anions and 8 other cations by intermolecular interactions. In **TM281** the cation is linked to the anion by a hydrogen bond O21–H21O⋯O3 (1.92 Å) (Fig. 8a). These dimers make chains along the a axis by C24–H24⋯O1 (2.40 Å), C124–H124⋯O2 (2.42 Å) and C10–H10⋯O3 (2.68 Å) intermolecular interactions (Fig. 8b). These chains propagate along the b axis by C114–H114⋯O22 (2.63 Å) and C126–H126⋯F2 (2.61 Å) intermolecular contacts (Fig. 8c). The packing is completed by the expansion of these building blocks along the c axis that are linked by the interactions C7–H7⋯O22 (2.45 Å), C21–H21⋯O2 (2.458 Å), C3–H3⋯F1 (2.60 Å) and C125–H125⋯π (centroid of the carboxylic group) (3.03 Å) (Fig. 8d).
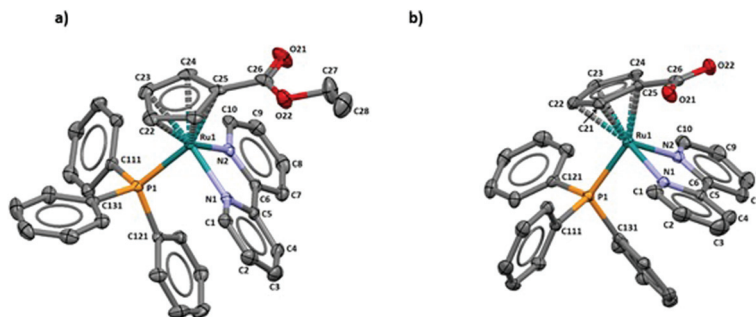
Fig. 6 Molecular diagrams depicting the cationic moieties for complexes [Ru(η^5-C$_5$H$_4$COOCH$_2$CH$_3$)(PPh$_3$)(2,2'-bipy)][CF$_3$SO$_3$], **3** (a) and [Ru(η^5-C$_5$H$_4$COOH)(PPh$_3$)(2,2'-bipy)][CF$_3$SO$_3$], **TM281** (b). Hydrogen atoms were omitted for clarity.
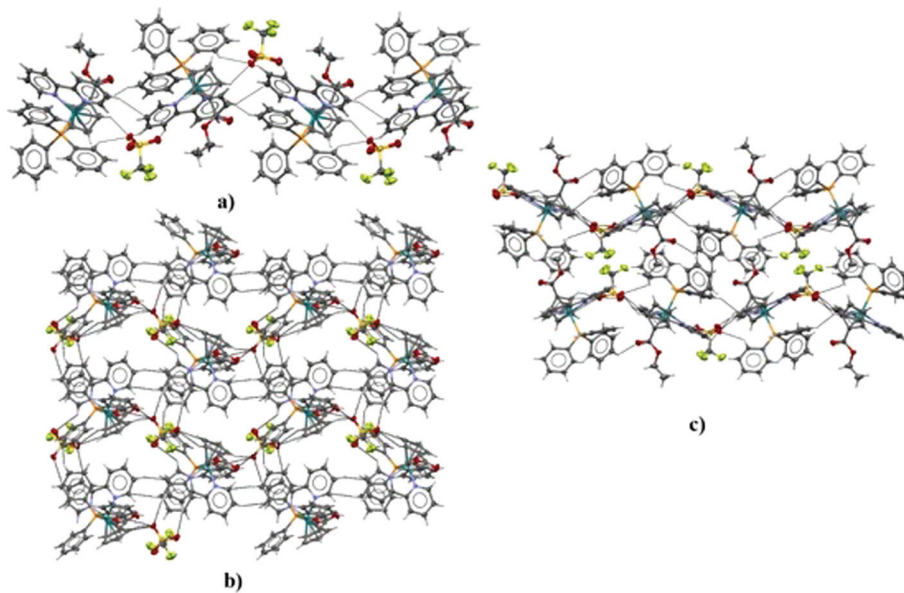

Fig. 7 Crystal lattice of **3**, (a) chains of cations intercalated with anions that grow along b; (b) expansion of chains along a; (c) overall packing.
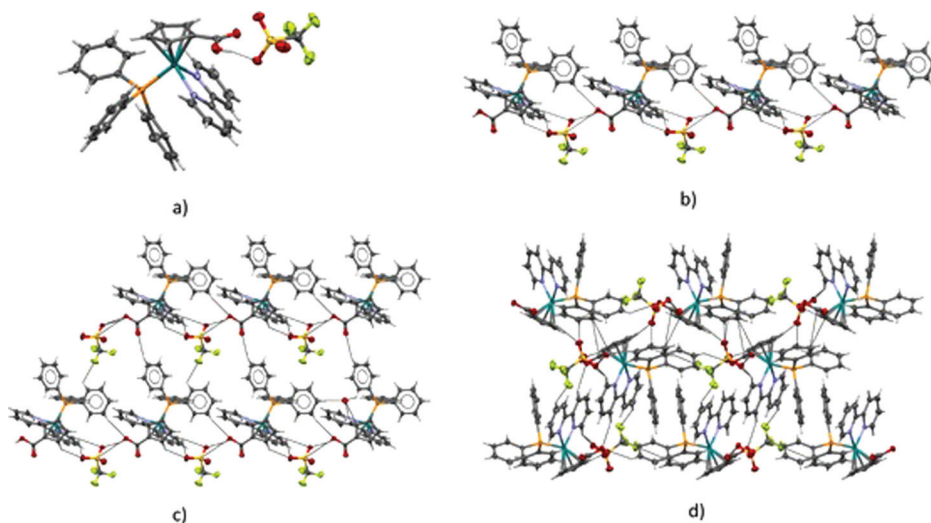

Fig. 8 Crystal packing of **TM281**, (a) a dimer of the cation and anion; (b) chains of dimers along a; (c) growth of chains along b; (d) overall packing.

Syntheses and characterization of the Ru(II)–peptide conjugates

The synthesis of the three new ruthenium–peptide conjugates **RuPC1**, **RuPC2** and **RuPC3** involved three main steps: (i) synthesis of the ruthenium organometallic starting material [Ru(η^5-C$_5$H$_4$COOH)(PPh$_3$)(2,2′-bipy)][CF$_3$SO$_3$] (**TM281**) described above, (ii) synthesis of the three peptides (**Pep1**, **Pep2** and **Pep3**) and (iii) conjugation of the organometallic precursor to the corresponding peptide. **Pep-1** was synthesized on an automatic assisted solid phase peptide microwave synthesizer (CEM Liberty), **Pep-2** and **Pep-3** were synthesized manually after several failed attempts using the automated process. Independent of the synthetic approach the general procedure for **RuPC1–RuPC3** is presented in Scheme 2. The organometallic starting material [Ru(η^5-C$_5$H$_4$COOH)(PPh$_3$)(2,2′-bipy)][CF$_3$SO$_3$] was chosen due to the existence of one carboxylic acid group appended to the cyclopentadienyl ring which is adequate for the condensation reaction with the terminal amino group of the peptides. Peptides **Pep-1**–**Pep-3** were synthesized on a Rink amide resin using standard Fluorenylmethyloxycarbonyl (Fmoc)-based solid-phase peptide synthesis. After peptide assembly on the resin, the terminal Fmoc was removed and the spacer 12-(9-fluorenylmethyloxycarbonylamino)-4,7,10-trioxa-dodecanoic acid (Fmoc-NH-PEG$_3$-COOH) was conjugated to the N-terminal using standard coupling reagents (HBTU/DIPEA in DMF). After Fmoc deprotection, the precursor complex **TM281** was conjugated manually using also a standard procedure described in the Experimental section. The Fmoc groups at the N-terminal of the resulting PEG(3)-peptides were removed and then the complex [Ru(η^5-C$_5$H$_4$COOH)(PPh$_3$)(2,2′-bipy)][CF$_3$SO$_3$] (**TM281**) was manually coupled, with 2-fold excess, in the presence of an equivalent amount of HBTU and 4-fold excess of DIPEA, in DMF. Peptide resins were N-deblocked with piperidine/DMF (20% v/v), followed by full deprotection and cleavage with TFA/H$_2$O/TIS (95 : 2.5 : 2.5 v/v, 2 h, RT) to give the ruthenium–peptide conjugates (see Scheme 2, and Fig. S19† for structures). All HPLC-purified ruthenium-peptide conjugates were satisfactorily characterized for purity by analytical HPLC (all three ruthenium-peptide conjugates were above 98% pure) and identified by ESI-MS (see Table S6 and Fig. S20–S25, ESI†).

Stability studies in DMSO and DMSO/DMEM

The stability in DMSO and 5%DMSO/DMEM + GlutaMAX-It cellular medium was also evaluated by UV-vis spectroscopy for all compounds. No significant changes were observed in the UV-vis spectra, indicating that all the complexes are air-stable in this solution (Fig. S26, ESI†).

Cytotoxicity in human breast cancer cells

The cytotoxic activity of **RuPCs 1–3**, the free peptides and their organometallic precursor was evaluated in the human FGFR(+) SKBR3 and FGFR(−) MDAMB231 breast cancer cells by the MTT assay. The parent compound **TM34** ([Ru(η^5-C$_5$H$_5$)(PPh$_3$)(2,2′-bipy)][CF$_3$SO$_3$]) was also evaluated for comparison. As can be observed in Fig. 9, in both cancer cells the presence of –COOH in the cyclopentadienyl ring in **TM281** led to a significant decrease of the cytotoxicity when compared with **TM34**. Probably this loss of activity may be explained by the weak acidic behaviour of the carboxylic acid function. Several inorganic and organometallic complexes with heteroaromatic carboxylic acids have been reported to show pK_a values
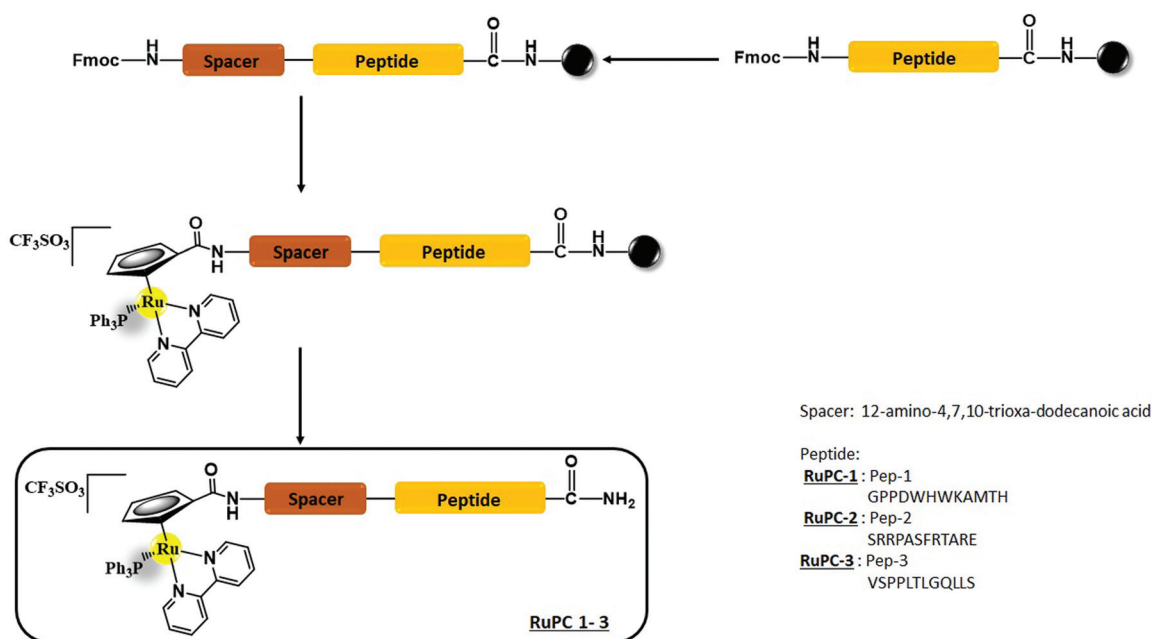
Scheme 2 Reaction scheme for the syntheses of Ru-peptide complexes (**RuPC1–RuPC3**). Spacer: 12-amino-4,7,10-trioxa-dodecanoic acid; peptide: **Pep1** (**RuPC1**), **Pep2** (**RuPC2**) and **Pep3** (**RuPC3**), ● resin.

≤5.[42–44] It is thus expected that the carboxylic acid group is primarily ionised at the physiological pH value. The carboxylate anion reduces the overall lipophilicity of the complex and provides a negative charge that is repelled by the anionic phospholipids commonly overexposed in the surface of the membrane of cancer cells.[45] Both factors cumulatively contribute to reducing the ability of **TM281** to be embedded in the phospholipid bilayer, where **TM34** acts.[27] The conjugation of the peptides to **TM281** leads to a decrease in the cytotoxicity when compared with the parent compound **TM281** at higher concentrations tested, 50 and 100 μM. This decrease in activity could be again explained by the increased hydrophilicity of the complexes caused by the introduction of the peptides. This effect of loss of activity as the hydrophilic character increases has already been observed for another **TM34** analogue, namely **TM85**, in which the introduction of a sulphonated group on the phosphane led to a substantial decrease in cytotoxicity.[30,46]

The conjugation of the peptides to **TM281** aimed to target the cells that express the FGRF receptors. In fact, the results showed (Fig. 9 and 10) that the conjugates are more cytotoxic towards SKBR cells that overexpress the FGFR receptors (7.7%, 24.7% and 26.5%, respectively for **RuPC1** to **RuPC3**), while for the organometallic compounds **TM281** and **TM34** no changes in cytotoxicity were observed for both cell lines. Cytotoxicity studies of the free peptides *per se* were also per-
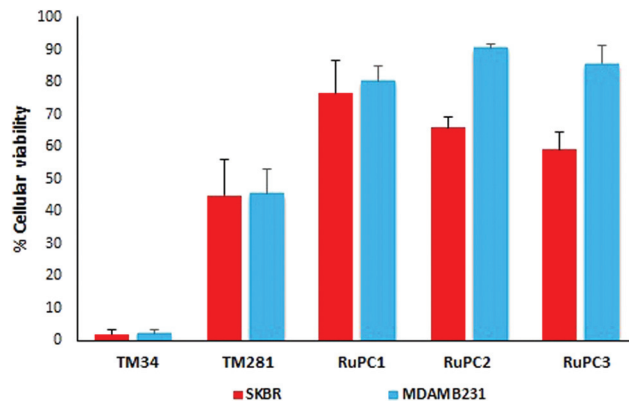
Fig. 10 Comparison of cell viability of **RuPC1**, **RuPC2**, **RuPC3**, **TM281** and **TM34** in the FGFR(+) SKBR3 and FGFR(−) MDAMB231 human breast cancer cells at 100 μM (48 h, 37 °C).

formed within the concentration range of 1–100 μM and did not reveal any effects. **RuPC2** and **RuPC3** peptides specific for receptor subtypes FGFR2 and FGFR3 were the most cytotoxic in SKBR3 cells. Despite the loss of activity, these results give an indication that this could be a promising approach to increase the selectivity towards different types of cancer cells that overexpress these receptors and above all to reduce the toxicity and non-selectivity observed for **TM34**. However, these results suggest that some chemical modifications to the group attached in the cyclopentadienyl ring are mandatory in order to increase the cytotoxic effect while retaining the selectivity for triple negative FGFR(+) breast cancer cells.

Experimental

Computational methods

Molecular dynamics (MD) simulations were performed to study the interaction of the **TM34** ruthenium complex with a lipid bilayer. The system was prepared with the complex placed in the water phase. A previously equilibrated membrane of 128 1,2-dimyristoyl-*sn-glycero*-3-phosphocholine (DMPC) solvated with ~4000 water molecules was used to prepare all starting configurations. The simulations were carried out using the GROMACS 2018.6 package[47] and the GROMOS 54A7 force field,[48] together with the SPC water model.[49] The topology for **TM34** was obtained by submitting several fragments to the Automated Topology Builder and Repository,[50] following a final construction and manual curation of the parameters. The atomic partial charges were obtained from a RESP fitting protocol.[51] The electrostatic potential was calculated with Gaussian 09[52] using the B3LYP functional[53–55] and the 6-31G** basis set[56] for all compounds with the exception of ruthenium, which used the Stuttgart/Dresden effective core potential basis set.[57]

The conformations were sampled according to an NPT ensemble where the pressure (1 bar; coupling constant of 2 ps)
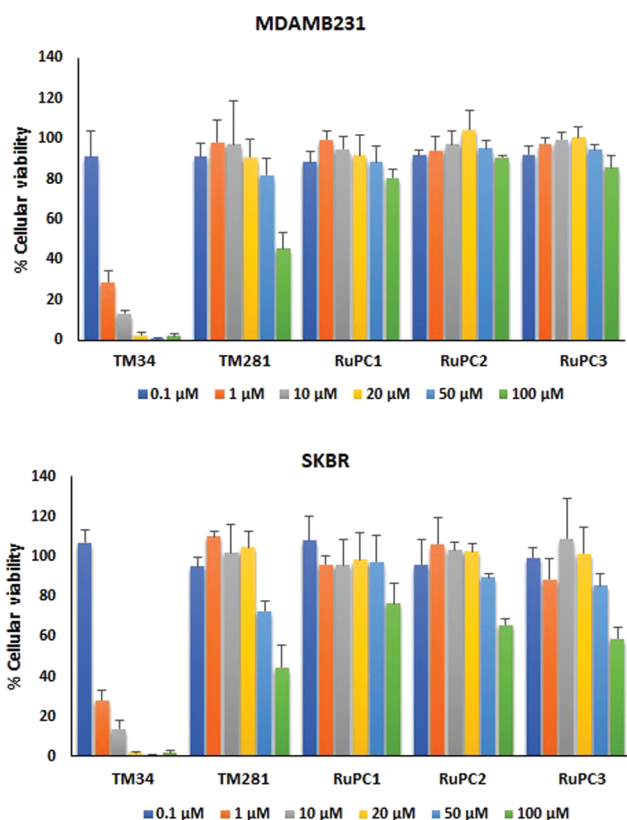
Fig. 9 Effect of **RuPC1**, **RuPC2**, **RuPC3**, **TM281** and **TM34** on the cellular viability of the FGFR(+) SKBR3 and FGFR(−) MDAMB231 human breast cancer cells (48 h, 37 °C).

and temperature (298 K; coupling constant of 0.1 ps) were kept constant using the Parrinello–Rahman barostat[58,59] and v-rescale thermostat,[60] respectively. Semi-isotropic pressure coupling was used with a compressibility of 4.5×10^{-5} bar^{-1}. The Particle mesh Ewald (PME) method with a real space cut-off of 1.0 nm and a Fourier grid spacing of 0.12 nm was used to deal with the electrostatic interactions. All van der Waals interactions were truncated above 1.0 nm. All bonds were constrained using the P-LINCS algorithm[61] for the membrane and **TM34** and SETTLE for water.[62] A 2 fs integration step was used, with the neighboring lists being updated every 10 steps. Minimization and initiation protocols were performed for all systems to avoid unfavorable interactions. In the minimization steps, the steepest descent and low-memory Broyden-Fletcher-Goldfarb-Shanno algorithms were used. The initiation was achieved in 2 MD simulation steps (100 ps each) with the membrane and **TM34** harmonically restrained in the first NVT step (restraint force: 1000 kJ mol^{-1} nm^{-2} and only the lipid bilayer restrained in the second NPT step. Five replicates were performed for 1 μs and the membrane insertion equilibrium was reached after 200 ns (initial segments were discarded in equilibrium analyses).

Membrane insertion analysis was performed by taking the average phosphorous atoms zz-position of the interacting monolayer as the zero reference. Positive values correspond to the water phase, while negative values correspond to the inserted regions, usually below the lipid phosphate groups. Pymol software (Schrödinger) was used for structure visualization and image rendering.

Materials and methods

All starting reagents and solvents were obtained from standard chemical suppliers. All manipulations involving air-free syntheses were carried out under a dinitrogen atmosphere using Schlenk techniques and the solvents used were dried by standard methods and freshly distilled before use. NMR spectra were recorded on a Bruker Avance 400 spectrometer at probe temperature (^{1}H NMR at 400 MHz, ^{13}C NMR at 100.6 MHz and ^{31}P NMR at 161.9 MHz). Chemical shifts (δ) were reported in parts per million (ppm) using CDCl$_3$ and $(CD_3)_2CO$ as solvents. [1]H and ^{13}C chemical shifts were measured relative to solvent peaks considering internal Me$_4$Si (0 ppm) and ^{31}P NMR was externally referenced to 85% H$_3$PO$_4$. Infrared spectra (4000–250 cm^{-1}) were recorded on a Thermo Nicolet 6700 spectrophotometer with KBr; only significant bands are cited in the text. Elemental analyses were performed at our laboratories (Laboratório de Análises, at Instituto Superior Técnico), using a Fisons Instruments EA1108 system. Data acquisition, integration and handling were performed using a PC with the software package EAGER-200 (Carlo Erba Instruments). Electronic spectra (range 220–900 nm) were recorded at room temperature on a Jasco V-660 spectrometer. Electrospray ionization mass spectrometry (ESI–MS) was performed on a QITMS instrument (Bruker HCT, Bruker, Billerica, MA, USA) in positive and negative ionization modes, using acetonitrile as solvent.

Ru(II) complex syntheses

Na(C$_5$H$_4$COOCH$_2$CH$_3$) 1. Na(C$_5$H$_4$COOCH$_2$CH$_3$) was prepared following the method described in the literature.[41] Freshly cracked cyclopentadiene (7 mL, 84.5 mmol) was added to a slurry of sodium sand (0.5 g, 21.3 mmol) in THF at 0 °C in a Schlenk flask. The mixture was magnetically stirred until all the sodium had reacted. Diethyl carbonate (19 mL, 112.6 mmol) was added to the resulting slightly pink solution of sodium cyclopentadienide. The mixture was stirred at room temperature for 10 min and then refluxed for 2 h. Then the solvent was removed under vacuum. The resulting solid was washed with diethyl ether until the filtrate was clear and then vacuum dried. Yield: 78%.

[Ru(η^5-C$_5$H$_4$COOCH$_2$CH$_3$)(PPh$_3$)$_2$Cl] 2. A solution of RuCl$_2$(PPh$_3$)$_3$ (2.4 g, 2.5 mmol) and Na(C$_5$H$_4$COOCH$_2$CH$_3$) **1** (0.4 g, 2.5 mmol) in 50 mL of THF was stirred at room temperature for 5 h. Addition of n-hexane (100 mL) produced an orange precipitate. The orange solid was cannula filtered, washed several times with n-hexane, and dried under vacuum. The product was recrystallized from dichloromethane/ n-hexane. Yield: 91%. ^{1}H NMR [CDCl$_3$, Me$_4$Si, δ/ppm]: 7.40 [m, 12, H$_{meta}$(PPh$_3$)], 7.22 [m, 6, H$_{para}$(PPh$_3$)], 7.11 [m, 12, H$_{ortho}$(PPh$_3$)], 4.91 [br, 2, Cp$_\beta$], 4.05 [q, 2, $\underline{CH_2}$CH$_3$, $^3J_{HH}$ = 7.02 Hz], 3.63 [br, 2, Cp$_\gamma$], 1.23 [t, 3, CH$_2\underline{CH_3}$, $^3J_{HH}$ = 7.34 Hz]. ^{13}C NMR [CDCl$_3$, δ/ppm]: 167.0 [C=O], 137.41 [Cq, PPh$_3$], 134.40 [CH, PPh$_3$], 128.95 [CH, PPh$_3$], 127.54 [CH, PPh$_3$], 86.90 [Cp$_\beta$], 83.75[Cp$_\alpha$],79.69 [Cp$_\gamma$], 60.65 [$\underline{CH_2}$CH$_3$], 14.41 [CH$_2\underline{CH_3}$]. ^{31}P NMR [CDCl$_3$, δ/ppm]: 37.38 [s, PPh$_3$]. FT-IR [KBr, cm^{-1}]: 3100–3049 cm^{-1} (ν_{C-H}, Cp and phenyl rings), 1708 cm^{-1} (ν(C=O)), 1479–1431 cm^{-1} ($\nu_{C=C}$, phenyl rings). This compound was found to be very sensitive to temperature decomposing at ≈60 °C.

[Ru(η^5-C$_5$H$_4$COOCH$_2$CH$_3$)(PPh$_3$)(2,2′-bipy)][CF$_3$SO$_3$] 3. To a stirred solution of [Ru(η^5-C$_5$H$_4$COOCH$_2$CH$_3$)(PPh$_3$)$_2$Cl] **2** (0.39 g, 0.5 mmol) in methanol (25 mL) was added 2,2′-bipyridine (0.10 g, 0.5 mmol) and AgCF$_3$SO$_3$ (0.13 g, 0.5 mmol). After refluxing for 5 h the solution turned from orange to red. The solution was separated from the AgCl precipitate by cannula-filtration and the solvent was evaporated under vacuum. The product was washed with n-hexane (2 × 10 mL) affording red crystals after recrystallization from dichloromethane/diethyl ether. Yield: 97%. ^{1}H NMR [(CD$_3$)$_2$CO, Me$_4$Si, δ/ppm]: 9.43 [d, 2, H4, $^3J_{HH}$ = 5.07 Hz], 8.24 [d, 2, H1, $^3J_{HH}$ = 7.90 Hz], 7.97 [t, 2, H2, $^3J_{HH}$ = 7.90 Hz], 7.43 [m, 5, H3 + H$_{para}$(PPh$_3$)], 7.35 [m, 6, H$_{meta}$(PPh$_3$)], 7.11 [m, 6, H$_{ortho}$(PPh$_3$)], 5.64 [br, 2, Cp$_\beta$], 4.76 [br, 2, Cp$_\gamma$], 3.83 [q, 2, $\underline{CH_2}$CH$_3$, $^3J_{HH}$ = 6.58 Hz], 0.79 [t, 3, CH$_2\underline{CH_3}$, $^3J_{HH}$ = 7.01 Hz]. ^{13}C NMR [(CD$_3$)$_2$CO, δ/ppm]:166.32 [C=O], 157.71 [C5, 2,2′-bipy], 156.59 [C4, 2,2′-bipy], 138.01 [C2, 2,2′-bipy], 133.76 [CH, PPh$_3$], 132.05 [C5, 2,2′-bipy], 131.65 [Cq, PPh$_3$], 131.06 [CH, PPh$_3$], 129.54 [CH, PPh$_3$], 126.37 [C3, 2,2′-bipy], 124.30 [C1, 2,2′-bipy], 85.54 [Cp$_\beta$], 78.18 [Cp$_\alpha$], 77.71[Cp$_\gamma$], 60.66 [$\underline{CH_2}$CH$_3$], 14.48 [CH$_2\underline{CH_3}$]. ^{31}P NMR [(CD$_3$)$_2$CO, δ/ppm]: 49.68 [s, PPh$_3$]. FT-IR [KBr, cm^{-1}]: 3100–3050 cm^{-1} (ν_{C-H}, Cp and phenyl rings), 1703 cm^{-1} (ν(C=O)), 1478–1419 cm^{-1} ($\nu_{C=C}$, phenyl rings), 1263 cm^{-1}

($\nu(CF_3SO_3)$). Elemental analysis (%) found: C, 54.7; H, 4.0; N, 3.4; S, 4.0. Calcd for $C_{37}H_{32}N_2PF_3O_5SRu\cdot0.1CH_2Cl_2$ (814.26): C, 54.72; H, 3.98; N, 3.44; S, 3.98.

[Ru(η^5-C$_5$H$_4$COOH)(PPh$_3$)(2,2′-bipy)][CF$_3$SO$_3$] TM281. A solution of [Ru(η^5-C$_5$H$_4$COOCH$_2$CH$_3$)(PPh$_3$)(2,2′-bipy)][CF$_3$SO$_3$] **3** (0.287 g, 0.356 mmol) and potassium carbonate (0.34 g, 2.46 mmol) in CH$_3$CN/H$_2$O (50 mL) was stirred at room temperature for 10 minutes and then refluxed under nitrogen for 6 h. The pH of the solution was brought to 1–2 by the addition of an ion exchange resin Amberlite®. The solution was collected by filtration, and the compound extracted with dichloromethane. The organic phases were collected and treated with anhydrous sodium sulfate. The solvents were removed by vacuum, and the product was washed with *n*-hexane (2 × 10 mL) affording red crystals after recrystallization from dichloromethane/diethyl ether. Yield: 95%. ^{1}H NMR [(CD$_3$)$_2$CO, Me$_4$Si, δ/ppm]: 9.43 [d, 2, H4, $^3J_{HH}$ = 5.62 Hz], 8.22 [d, 2, H1, $^3J_{HH}$ = 8.17 Hz], 7.95 [t, 2, H2, $^3J_{HH}$ = 7.94 Hz], 7.44 [m, 5, H3 + H$_{para}$(PPh$_3$)], 7.34 [m, 6, H$_{meta}$(PPh$_3$)], 7.12 [m, 6, H$_{ortho}$(PPh$_3$)], 5.60 [br, 2, Cp$_\beta$], 4.78 [br, 2, Cp$_\gamma$]. ^{13}C NMR [(CD$_3$)$_2$CO, δ/ppm]: 167.67 [C=O], 157.11 [C5, 2,2′-bipy], 156.61 [C4, 2,2′-bipy], 137.84 [C2, 2,2′-bipy], 133.80 [CH, PPh$_3$], 131.68 [Cq, PPh$_3$], 131.24 [CH, PPh$_3$], 129.42 [CH, PPh$_3$], 126.63 [C3, 2,2′-bipy], 124.24 [C1, 2,2′-bipy], 85.65 [Cp$_\beta$], 78.69 [Cp$_\alpha$], 77.92 [Cp$_\gamma$]. ^{31}P NMR [(CD$_3$)$_2$CO, δ/ppm]: 49.72 [s, PPh$_3$]. FT-IR [KBr, cm^{-1}]: 3100–3040 cm^{-1} (ν_{C-H}, Cp and phenyl rings and ν_{O-H}), 1701 cm^{-1} (ν(C=O)), 1478–1421 cm^{-1} ($\nu_{C=C}$, phenyl rings), 1284 cm^{-1} ($\nu(CF_3SO_3)$). Elemental analysis (%) found: C, 53.8; H, 3.5; N: 3.5; S, 4.0. Calcd for $C_{35}H_{28}N_2PF_3O_5SRu\cdot0.1CH_2Cl_2$ (786.20): C, 53.62; H, 3.61; N: 3.56; S, 4.07.

Ru(II)–peptide conjugate syntheses

The peptides **Pep1**, **Pep2** and **Pep3** were synthesized as C-terminal amides using standard 9-fluorenylmethyloxycarbonyl (Fmoc) solid phase synthesis methods. Automated synthesis of **Pep-1** was performed using a microwave-assisted Liberty 1 Peptide Synthesizer (CEM, Matthews, NC), running standard protocols at the 0.1 mmol scale on Rink amide MBHA resin. Fivefold excess of Fmoc-L-amino acids and HBTU, in the presence of 10-fold excess of DIPEA, were used for the coupling steps in DMF. All side-chain functions were protected with TFA labile groups. **Pep2** and **Pep3** were manually synthesized using the same stoichiometry of Fmoc-L-amino acids, HBTU and DIPEA. Removal of the Fmoc group for amino acid terminal deprotection, at each conjugation step, was performed with a piperidine/DMF (20% v/v) solution.

A spacer, 12-(9-fluorenylmethyloxycarbonylamino)-4,7,10-trioxa-dodecanoic acid (Fmoc-NH-PEG$_3$-COOH), was coupled manually to each peptide, with 2-fold excess, in the presence of an equivalent amount of HBTU and 4-fold excess of DIPEA, in DMF, followed by the manual coupling of the complex [Ru (η^5-C$_5$H$_4$COOH)(PPh$_3$)(2,2′-bipy)][CF$_3$SO$_3$] (**TM281**), in 2-fold excess, in the presence of an equivalent amount of HBTU and 4-fold excess of DIPEA, in DMF. After the synthesis completed, peptide resins were treated with piperidine/DMF (20% v/v) to remove the Fmoc group, followed by treatment with TFA/H$_2$O/ TIS (95 : 2.5 : 2.5 v/v, 2 h, RT) to promote full deprotection and cleavage from the resin. Ru–peptide conjugates precipitated by addition of ice-cold diethyl ether and were then dissolved in water, purified by HPLC and lyophilized. Analytical reverse-phase HPLC was performed on C18 columns (4.6 × 250 mm, 5 μm, Supelco Analytical 568223-U) using a PerkinElmer Series 200® instrument coupled to a PerkinElmer Series 200® degasser and a PerkinElmer Series 200® UV-vis detector. Solvent A was 0.1% (v/v) TFA in water, and solvent B 0.1% (v/v) TFA in acetonitrile. Elution was done with linear gradients of solvent B into A over 25 minutes at a 2 mL min^{-1} flow rate, with UV detection at 220 nm. Preparative reverse-phase HPLC was performed on a C18 column (8 × 250 mm, 7 μm, Macherey-Nagel VP250/8 Nucleosil 100-7®) in a model Waters 2535® coupled with a Uniflows DG-3210® degasser and a Waters 2998® UV-vis detector. Solvents A and B were 0.1% TFA (v/v) in water and acetonitrile, respectively, and elution was again with linear gradients of solvent B into solvent A over 45 minutes, at a 1 mL min^{-1} flow rate, with UV detection at 220 nm. Preparative fractions of satisfactory purity (≥95%, determined by analytical HPLC) were collected and lyophilized.

Electrochemical studies

Cyclic voltammograms were obtained at room temperature using an EG&G Princeton Applied Research Potentiostat/ Galvanostat Model 273A equipped with Electrochemical PowerSuite v2.51 software for electrochemical analysis, in anhydrous dichloromethane or acetonitrile with tetrabutyl-ammonium hexafluorophosphate (0.2 and 0.1 M respectively) as the supporting electrolyte. The electrochemical cell was a homemade three electrode configuration cell with a platinum-disc working electrode (1.0 mm) probed by a Luggin capillary connected to a silver-wire pseudo-reference electrode and a platinum wire auxiliary electrode. All the potentials reported were measured against the ferrocene/ferrocenium redox couple as the internal standard and normally quoted relative to SCE (using the ferrocenium/ferrocene redox couple $E_{1/2}$ = 0.46 or 0.40 V *versus* SCE for dichloromethane or acetonitrile respectively.

Both the sample and the electrolyte (Fluka) were dried under vacuum for several hours prior to the experiment. Reagent grade solvents were dried, purified by standard procedures and distilled under a nitrogen atmosphere before use. All the experiments were performed in an oxygen-free and moisture-free atmosphere.

X-ray crystal structure determination

Crystals of **3** and **TM281**, suitable for the X-ray diffraction study, were mounted on a loop with Fomblin© protective oil for data collection. Data were collected on a Bruker AXS-KAPPA APEX II diffractometer with graphite-monochromated radiation (Mo Kα, λ = 0.17069 Å) at 150 K. The X-ray generator was operated at 50 kV and 30 mA, and X-ray data collection was monitored using the APEX program.[63] Empirical absorption correction using SADABS[64] was applied and data reduction was done with the SAINT program.[65] SHELXS[66] was used for

structure solution, and SHELXL[66] was used for full matrix least-squares refinement on F^2. Both programs are included in the package of programs WINGX-Version 2014.1.[67] Non-hydrogen atoms were refined anisotropically. All hydrogen atoms were inserted in calculated positions and allowed to refine in the parent carbon atom. The hydrogen bonds and intermolecular interactions were calculated using PLATON.[68] Graphical representations were prepared using MERCURY 3.8.[69] A summary of the crystal data, structure solution and refinement parameters for the structures is provided in Table S7.†

Cytotoxicity assays

Human breast cancer cell lines, SKBR3 (ATCC) and MDAMB231 (ATCC), were cultured in DMEM + Glutamax-I (Gibco) supplemented with 10% fetal bovine serum (FBS) and 1% antibiotics. Cells were cultured in an incubator (Heraeus, Germany) with a humidified atmosphere at 5% CO_2, 37 °C. Cell viability was evaluated using the MTT ([3-(4,5-dimethylthiazol-2-yl)-2,5-diphenyltetrazolium bromide]) assay which is based on the reduction of the tetrazolium salt to purple formazan by a mitochondrial dehydrogenase in metabolically active cells. For the assays, the cells were seeded in 96-well plates (2–3 × 10^4 cells/200 μL) and allowed to adhere overnight. The Ru complexes were first solubilized in DMSO and then in the medium to prepare working solutions in the range 0.1 μM–100 μM. The peptides were first diluted in water and then in the medium and assayed using the same concentration range. After continuous exposure to the compounds for 48 h at 37 °C, the medium was removed, and the cells were incubated with 200 μL of the MTT solution (0.5 mg mL^{-1}) for 3 h. Then, the solution was discarded and the purple formazan inside the cells was dissolved in 200 μL of DMSO. Cellular viability was evaluated by measuring the absorbance at 570 nm on a plate spectrophotometer (PowerWave Xs, Bio-Tek Instruments, Winooski, VT, USA). The cytotoxic effect of the compounds was quantified by calculating the IC_{50} using GraphPad Prism software (vs. 5.0). All compounds were tested in at least two independent experiments, each comprising six replicates per concentration.

Conclusions

Molecular dynamics simulations of the complex [RuCp(PPh$_3$)(2,2′-bipy)][CF$_3$SO$_3$] **TM34** with a phosphatidylcholine bilayer membrane model showed that derivatizations on either Cp or 2,2′-bipy ligands should not perturb the membrane interaction abilities of the **TM34** derivatives. Hence, three new complexes, [Ru(η^5-C$_5$H$_4$**COOCH$_2$CH$_3$**)(PPh$_3$)$_2$Cl] **2**, [Ru(η^5-C$_5$H$_4$**COOCH$_2$CH$_3$**) (PPh$_3$)(2,2′-bipy)][CF$_3$SO$_3$] **3**, and [Ru(η^5-C$_5$H$_4$**COOH**)(PPh$_3$)(2,2′-bipy)][CF$_3$SO$_3$] **TM281**, with functionalized cyclopentadienyl rings have been synthesized and fully characterized and the X-ray structures of **3** and **TM281** were determined. These complexes have the common feature of the Cp ring functionalized with carboxyl substitu-

ents and constitute a barely studied family of piano stool structured complexes. The syntheses of such compounds were achievable due to the improvement made here by the conversion of esters into carboxylic acids by use of an ion exchange resin, instead of acidification using strong acids, as generally described in the literature.

These half-sandwich ruthenium(ii)-cyclopentadienyl complexes of general formula [Ru(η^5-C$_5$H$_4$**CO$_2$H**)(η^2-L)L′]X were revealed to be the adequate starting materials to react with biomolecules, in particular peptides, to afford a novel family of Ru-peptide conjugates with biological potential to act as anticancer agents.

To the best of our knowledge, these are the first half-sandwich ruthenium(ii)-cyclopentadienyl peptide conjugates reported in the literature. The cytotoxicity of RuPCs was evaluated in the human FGFR(+) SKBR3 and FGFR(−) MDAMB231 breast cancer cells. Under the same experimental conditions, it was observed that the presence of –COOH in the cyclopentadienyl ring in **TM281** led to a significant decrease in the cytotoxicity when compared with **TM34**, probably due to acid ionization, which reduces the ability of **TM281** to be embedded in the phospholipid bilayer, where **TM34** acts. Nevertheless, ruthenium–peptide conjugates are more cytotoxic towards SKBR3 cells that overexpress the FGFR receptors than MDAMD231 (FGFR−), indicating that, although some chemical modifications to the group attached to the Cp are mandatory in order to increase the cytotoxicity, this is a promising approach for selectively targeting FGFR(+) breast cancer cells.

Conflicts of interest

There are no conflicts to declare.

Acknowledgements

Notes and references

1 Cancer, https://www.who.int/news-room/fact-sheets/detail/cancer (accessed 22 November 2019).

2 Burden of breast cancer by numbers, https://www.roche.com/dam/jcr:fd833dba-1d27-44dd-8261-6a490e7f5fe9/en/infographic_breast_cancer_by_numbers.pdf (accessed 22 November 2019).

3 World cancer factsheet, World cancer burden, https://www.cancerresearchuk.org/sites/default/files/cs_report_world.pdf (accessed 22 November 2019).

4 M. E. Reyes, T. Fujii, D. Branstetter, S. Krishnamurthy, H. Masuda, X. Wang, J. M. Reuben, W. A. Woodward, B. J. Edwards, G. N. Hortobagyi, D. Tripathy, W. C. Dougall, B. L. Eckhardt and N. T. Ueno, *Breast Cancer Res. Treat.*, 2017, **164**, 57–67.

5 A. Urruticoechea, R. Alemany, J. Balart, A. Villanueva, F. Vinals and G. Capella, *Curr. Pharm. Des.*, 2010, **16**, 3–10.

6 D. W. Hoskin and A. Ramamoorthy, *Biochim. Biophys. Acta, Biomembr.*, 2008, **1778**, 357–375.

7 C. Soussain, D. Ricard, J. R. Fike, J. J. Mazeron, D. Psimaras and J. Y. Delattre, *Lancet*, 2009, **374**, 1639–1651.

8 N. Papo and Y. Shai, *Cell. Mol. Life Sci.*, 2005, **62**, 784–790.

9 P. J. Loehrer and L. H. Einhorn, *Ann. Intern. Med.*, 1984, **100**, 704–713.

10 A. A. Nazarov, J. Risse, W. H. Ang, F. Schmitt, O. Zava, A. Ruggi, M. Groessl, R. Scopelitti, L. Juillerat-Jeanneret, C. G. Hartinger and P. J. Dyson, *Inorg. Chem.*, 2012, **51**, 3633–3639.

11 K. Lin, Z. Z. Zhao, H. Ben Bo, X. J. Hao and J. Q. Wang, *Front. Pharmacol.*, 2018, **9**, 1323.

12 G. Sava, S. Pacor, A. Bergamo, M. Cocchietto, G. Mestroni and E. Alessio, *Chem.-Biol. Interact.*, 1995, **95**, 109–126.

13 E. Alessio and L. Messori, *Molecules*, 2019, **24**, 1995.

14 M. Gras, B. Therrien, G. Süss-Fink, O. Zava and P. J. Dyson, *DaltonTrans.*, 2010, **39**, 10305–10313.

15 C. S. Allardyce, P. J. Dyson, D. J. Ellis and S. L. Heath, *Chem. Commun.*, 2001, 1396–1397.

16 L. A. Huxham, E. L. S. Cheu, B. O. Patrick and B. R. James, *Inorg. Chim. Acta*, 2003, **352**, 238–246.

17 R. E. Morris, R. E. Aird, P. Del Socorro Murdoch, H. Chen, J. Cummings, N. D. Hughes, S. Parsons, A. Parkin, G. Boyd, D. I. Jodrell and P. J. Sadler, *J. Med. Chem.*, 2001, **44**, 3616–3621.

18 M. H. Garcia, T. S. Morais, P. Florindo, M. F. M. Piedade, V. Moreno, C. Ciudad and V. Noe, *J. Inorg. Biochem.*, 2009, **103**, 354–361.

19 V. Moreno, J. Lorenzo, F. X. Aviles, M. H. Garcia, J. P. Ribeiro, T. S. Morais, P. Florindo and M. P. Robalo, *Bioinorg. Chem. Appl.*, 2010, 936834.

20 T. S. Morais, A. Valente, A. I. Tomaz, F. Marques and M. H. Garcia, *Future Med. Chem.*, 2016, **8**, 527–544.

21 T. S. Morais, T. J. L. Silva, F. Marques, M. P. Robalo, F. Avecilla, P. J. A. Madeira, P. J. G. Mendes, I. Santos and M. H. Garcia, *J. Inorg. Biochem.*, 2012, **114**, 65–74.

22 M. H. Garcia, A. Valente, P. Florindo, T. S. Morais, M. F. M. Piedade, M. T. Duarte, V. Moreno, F. X. Avilés and J. Loreno, *Inorg. Chim. Acta*, 2010, **363**, 3765–3775.

23 L. Côrte-Real, R. G. Teixeira, P. Gírio, E. Comsa, A. Moreno, R. Nasr, H. Baubichon-Cortay, F. Avecilla, F. Marques, M. P. Robalo, P. Mendes, J. P. P. Ramalho, M. H. Garcia, P. Falson and A. Valente, *Inorg. Chem.*, 2018, **57**, 4629–4639.

24 R. G. Teixeira, A. R. Brás, L. Côrte-Real, R. Tatikonda, A. Sanches, M. P. Robalo, F. Avecilla, T. Moreira, M. H. Garcia, M. Haukka, A. Preto and A. Valente, *Eur. J. Med. Chem.*, 2018, **143**, 503–514.

25 L. Côrte-Real, M. P. Robalo, F. Marques, G. Nogueira, F. Avecilla, T. J. L. Silva, F. C. Santos, A. I. Tomaz, M. H. Garcia and A. Valente, *J. Inorg. Biochem.*, 2015, **150**, 148–159.

26 L. Côrte-Real, A. P. Matos, I. Alho, T. S. Morais, A. I. Tomaz, M. H. Garcia, I. Santos, M. P. Bicho and F. Marques, *Microsc. Microanal.*, 2013, **19**, 1122–1130.

27 L. Côrte-Real, F. Mendes, J. Coimbra, T. S. Morais, A. I. Tomaz, A. Valente, M. H. Garcia, I. Santos, M. Bicho and F. Marques, *J. Biol. Inorg. Chem.*, 2014, **19**, 853–867.

28 T. S. Morais, F. Santos, L. Côrte-Real, F. Marques, M. P. Robalo, P. J. A. Madeira and M. H. Garcia, *J. Inorg. Biochem.*, 2013, **122**, 8–17.

29 A. I. Tomaz, T. Jakusch, T. S. Morais, F. Marques, R. F. M. De Almeida, F. Mendes, É. A Enyedy, I. Santos, J. C. Pessoa, T. Kiss and M. H. Garcia, *J. Inorg. Biochem.*, 2012, **117**, 261–269.

30 T. S. Morais, F. C. Santos, T. F. Jorge, L. Côrte-Real, P. J. A. Madeira, F. Marques, M. P. Robalo, A. Matos, I. Santos and M. H. Garcia, *J. Inorg. Biochem.*, 2014, **130**, 1–14.

31 N. Mendes, F. Tortosa, A. Valente, F. Marques, A. Matos, T. Morais, A. Tomaz, F. Gärtner and M. Garcia, *Anticancer Agents Med. Chem.*, 2016, **16**, 1–1.

32 C. S. Burke, A. Byrne and T. E. Keyes, *Angew. Chem., Int. Ed.*, 2018, **57**, 12420–12424.

33 A. A. Kaspar and J. M. Reichert, *Drug Discovery Today*, 2013, **18**, 807–817.

34 D. P. Perrault, G. K. Lee, S. Y. Park, S. Lee, D. Choi, E. Jung, Y. J. Seong, E. K. Park, C. Sung, R. Yu, A. Bouz, A. Pourmoussa, S. J. Kim, Y. K. Hong and A. K. Wong, *LymphaticRes.Biol.*, 2019, **17**, 19–29.

35 M. Mohammadi, S. K. Olsen and O. A. Ibrahimi, *Cytokine Growth Factor Rev.*, 2005, **16**, 107–137.

36 J. Perez-Garcia, E. Muñoz-Couselo, J. Soberino, F. Racca and J. Cortes, *Breast*, 2018, **37**, 126–133.

37 V. Moreno, M. Font-Bardia, T. Calvet, J. Lorenzo, F. X. Avilés, M. H. Garcia, T. S. Morais, A. Valente and M. P. Robalo, *J. Inorg. Biochem.*, 2011, **105**, 241–249.

38 M. Jin, Y. Yu, H. Qi, Y. Xie, N. Su, X. Wang, Q. Tan, F. Luo, Y. Zhu, Q. Wang, X. Du, C. J. Xian, P. Liu, H. Huang, Y. Shen, C. X. Deng, D. Chen and L. Chen, *Hum. Mol. Genet.*, 2012, **21**, 5443–5455.

39 Q. Tan, B. Chen, Q. Wang, W. Xu, Y. Wang, Z. Lin, F. Luo, S. Huang, Y. Zhu, N. Su, M. Jin, C. Li, L. Kuang, H. Qi, Z. Ni, Z. Wang, X. Luo, W. Jiang, H. Chen, S. Chen, F. Li, B. Zhang, J. Huang, R. Zhang, K. Jin, X. Xu, C. Deng, X. Du, Y. Xie and L. Chen, *Osteoarthr. Cartil.*, 2018, **26**, 1733–1743.

40 J. Zhou, L. He, Z. Pang, H. D. Appelman, R. Kuick, D. G. Beer, M. Li and T. D. Wang, *Identification and validation of FGFR2 peptide for detection of early Barrett's neoplasia*, 2017.

41 W. P. Hart, D. Shihua and M. D. Rausch, *J. Organomet. Chem.*, 1985, **282**, 111–121.

42 P. H. Xie, Y. J. Hou, B. W. Zhang, Y. Cao, F. Wu, W. J. Tian and J. C. Shen, *J. Chem. Soc., Dalton Trans.*, 1999, 4217–4221.

43 C. H. Su, H. Y. Chen, K. Y. Da Tsai and I. J. Chang, *J. Phys. Chem. B*, 2007, **111**, 6857–6860.

44 M. G. Crisp, E. R. T. Tiekink and L. M. Rendina, *Inorg. Chem.*, 2003, **42**, 1057–1063.

45 A. C. Alves, D. Ribeiro, C. Nunes and S. Reis, *Biochim. Biophys. Acta, Biomembr.*, 2016, **1858**, 2231–2244.

46 L. Gano, T. Pinheiro, A. P. Matos, F. Tortosa, T. F. Jorge, M. S. Gonçalves, M. Martins, T. S. Morais, A. Valente, A. I. Tomaz, M. H. Garcia and F. Marques, *Anticancer Agents Med. Chem.*, 2019, **19**, 1262–1275.

47 S. Pronk, S. Páll, R. Schulz, P. Larsson, P. Bjelkmar, R. Apostolov, M. R. Shirts, J. C. Smith, P. M. Kasson, D. Van Der Spoel, B. Hess and E. Lindahl, *Bioinformatics*, 2013, **29**, 845–854.

48 N. Schmid, A. P. Eichenberger, A. Choutko, S. Riniker, M. Winger, A. E. Mark and W. F. Van Gunsteren, *Eur. Biophys. J.*, 2011, **40**, 843–856.

49 J. Hermans, H. J. C. Berendsen, W. F. Van Gunsteren and J. P. M. Postma, *Biopolymers*, 1984, **23**, 1513–1518.

50 K. B. Koziara, M. Stroet, A. K. Malde and A. E. Mark, *J. Comput.-Aided Mol. Des.*, 2014, **28**, 221–233.

51 C. I. Bayly, P. Cieplak, W. Cornell and P. A. Kollman, *J. Phys. Chem.*, 1993, **97**, 10269–10280.

52 M. J. Frisch, G. W. Trucks, H. B. Schlegel, G. E. Scuseria, M. A. Robb, J. R. Cheeseman, G. Scalmani, V. Barone, B. Mennucci, G. A. Petersson, H. Nakatsuji, M. Caricato, X. Li, H. P. Hratchian, A. F. Izmaylov, J. Bloino, G. Zheng, J. L. Sonnenberg, M. Hada, M. Ehara, K. Toyota, R. Fukuda, J. Hasegawa, M. Ishida, T. Nakajima, Y. Honda, O. Kitao, H. Nakai, T. Vreven, J. A. Montgomery, J. E. Peralta Jr., F. Ogliaro, M. Bearpark, J. J. Heyd, E. Brothers, K. N. Kudin, V. N. Staroverov, R. Kobayashi, J. Normand, K. Raghavachari, A. Rendell, J. C. Burant, S. S. Iyengar, J. Tomasi, M. Cossi, N. Rega, J. M. Millam, M. Klene, J. E. Knox, J. B. Cross, V. Bakken, C. Adamo, J. Jaramillo, R. Gomperts, R. E. Stratmann, O. Yazyev, A. J. Austin, R. Cammi, C. Pomelli, J. W. Ochterski, R. L. Martin, K. Morokuma, V. G. Zakrzewski, G. A. Voth, P. Salvador, J. J. Dannenberg, S. Dapprich, A. D. Daniels, Ö. Farkas, J. B. Foresman, J. V. Ortiz, J. Cioslowski and D. J. Fox, 2009.

53 A. D. Becke, *J. Chem. Phys.*, 1993, **98**, 5648–5652.

54 S. H. Vosko, L. Wilk and M. Nusair, *Can. J. Phys.*, 1980, **58**, 1200–1211.

55 C. Lee, W. Yang and R. G. Parr, *Phys. Rev. B: Condens. Matter Mater. Phys.*, 1988, **37**, 785–789.

56 P. C. Hariharan and J. A. Pople, *Theor. Chim. Acta*, 1973, **28**, 213–222.

57 M. Dolg, U. Wedig, H. Stoll and H. Preuss, *J. Chem. Phys.*, 1987, **86**, 866–872.

58 M. Parrinello and A. Rahman, *J. Appl. Phys.*, 1981, **52**, 7182–7190.

59 S. Nosé and M. L. Klein, *Mol. Phys.*, 1983, **50**, 1055–1076.

60 G. Bussi, D. Donadio and M. Parrinello, *J. Chem. Phys.*, 2007, **126**, 014101.

61 B. Hess, *J. Chem. Theory Comput.*, 2008, **4**, 116–122.

62 S. Miyamoto and P. A. Kollman, *J. Comput. Chem.*, 1992, **13**, 952–962.

63 *APEX2 v2009.3-0*, Bruker AXS Inc., Madison, Wisconsin, USA, 2009.

64 *SABADS: Area-detector Absorption Correction*, 2004.

65 A. I. S. (Version 7. 23. SAINT, 2004.

66 G. M. Sheldrick, *Acta Crystallogr., Sect. A: Found. Crystallogr.*, 2008, **64**, 112–122.

67 L. J. Farrugia, *J. Appl. Crystallogr.*, 2012, **45**, 849–854.

68 A. L. Spek, *Acta Crystallogr., Sect. D: Biol. Crystallogr.*, 2009, **65**, 148–155.

69 C. F. Macrae, P. R. Edgington, P. McCabe, E. Pidcock, G. P. Shields, R. Taylor, M. Towler and J. van de Streek, *J. Appl. Crystallogr.*, 2006, **39**, 453–457.